# Surface climate signals transmitted rapidly to deep North Atlantic throughout last millennium

Wanyi Lu<sup>1\*</sup>, Delia W. Oppo<sup>1</sup>, Geoffrey Gebbie<sup>1</sup>, David J. R. Thornalley <sup>1,2</sup>

\*Corresponding author. Email: wlu@whoi.edu

## **Abstract:**

Instrumental observations of subsurface ocean warming imply that ocean heat uptake has slowed 20<sup>th</sup>-century surface warming. We present high-resolution records from subpolar North Atlantic sediments that are consistent with instrumental observations of surface and deep warming/freshening and, in addition, reconstruct the surface-deep relation of the last 1,200 years. Sites from ~1300 meters and deeper suggest an ~ 0.5°C cooling across the Medieval Climate

Anomaly to Little Ice Age transition that began ~1350 ± 50 Common Era (CE), whereas surface records suggest asynchronous cooling onset spanning ~ 600 years. These data suggest that ocean circulation integrates surface variability that is transmitted rapidly to depth by the Atlantic Meridional Ocean Circulation, implying that the ocean moderated Earth's surface temperature throughout the last millennium as it does today.

## **One-Sentence Summary:**

Surface climate changes of the last 1,200 years were transferred rapidly to the deep North Atlantic.

25

5

<sup>&</sup>lt;sup>1</sup> Woods Hole Oceanographic Institution, Woods Hole, MA, USA

<sup>&</sup>lt;sup>2</sup> Department of Geography, University College London, London, UK

## **Main Text:**

5

10

15

20

25

30

35

40

45

Earth's surface has generally warmed over the last century (1), but the ocean has slowed this warming by taking up over 90% of the excess thermal energy since 1955 (2) and increasingly storing it in the deep oceans (3-5). Climate reconstructions provide a baseline for assessing the anomalous nature of twentieth century change and the role of the deep ocean in moderating surface climate on longer time scales. The Common Era (i.e., the last ~2,000 years, CE) contained significant climate variability, including a cooling trend from the peak of the Medieval Climate Anomaly (MCA, around 850-1250 CE) to the Little Ice Age (LIA, around 1400-1850 CE), and rapid industrial warming since  $\sim$ 1850 (1, 6). The high-latitude North Atlantic Ocean is an important region where deep water forms and surface temperature anomalies are expected to be transported efficiently to depth via the Atlantic Meridional Overturning Circulation (AMOC) (7). However, few high-resolution records from the deep North Atlantic span the MCA-LIA transition (8), and the hypothesis that an active AMOC moderated surface climate on centennial time scales across this transition has not been evaluated with deep North Atlantic proxy records. Here we present data from well-dated sediment cores that form a depth transect spanning ~1000-2300 m and sample several important water masses in the subpolar North Atlantic. These data permit us to compare changes in the properties of the Nordic Overflows to those of waters formed south of the Nordic Seas, and with the insights of a model, place aspects of modern ocean warming in a longer-term context.

We used 11 marine sediment cores from south of Iceland along the eastern flank of Reykjanes Ridge, collected in 2014 on the research vessel R/V Endeavor (cruise EN539) (Table S1, Fig. 1). Iceland Scotland Overflow (ISOW) entering the northern Iceland Basin is much denser than the ambient Atlantic intermediate waters near the sill depths (~500 – 800 m), resulting in vigorous mixing and entrainment, especially during its initial descent, but also as it flows along the flank of the Reykjanes Ridge (9). A water mass decomposition from an inversion of oceanographic data (Fig. S1-S2, (10)) indicates that all our core sites contain a mixture of ISOW, colder, fresher Labrador Sea Water (LSW), and warmer, saltier Subpolar Mode Water (SPMW). SPMW is most prevalent at the shallowest site, whereas the ISOW contribution increases with depth, reaching a maximum of nearly 60% at our deepest site. The LSW contribution is relatively constant with depth, with a maximum at about 1300 m. Higher seawater density north of the sills compared to south of them has largely driven the transport of overflow waters over the last century (11).

We measured the oxygen and carbon isotope ratios,  $\delta^{18}O$  and  $\delta^{13}C$  (the  $^{18}O/^{16}O$  and  $^{13}C/^{12}C$  in each sample, relative to that of an international standard), in two species of planktic foraminifera (*Globigerina bulloides*, which calcifies in the upper ~50 m (*12*), and *Globorotalia inflata*, which calcifies as deep as ~300 m (*13*)), and in one of two species of benthic foraminifera (*Cibicidoides wuellerstorfi* or *Uvigerina peregrina*), depending on their availability. Variations in the  $\delta^{18}O$  of foraminifera reflect variations in calcification temperature and the  $\delta^{18}O$  of seawater, the latter in turn influenced by salinity (*14*); foraminiferal  $\delta^{18}O$  increases with increasing seawater  $\delta^{18}O$  and with decreasing temperature. In addition, *C. wuellerstorfi* calcifies in equilibrium with seawater, but  $\delta^{18}O$  values in *U. peregrina* are ~0.47 % higher (*14*). In the modern subpolar North Atlantic below 1000 m (*15*), variations in the  $\delta^{18}O$  of calcite are largely due to temperature variability ( $R^2 = 0.93$ ) rather than salinity ( $R^2 = 0.00$ ) (Fig. S3), and modern measured benthic  $\delta^{18}O$  closely follows the predicted  $\delta^{18}O$  of calcite (Fig. S2). Chronologies and their uncertainties were constrained by radiocarbon data and determined using Bayesian methods (*16*) (Methods). All cores have high sediment accumulation rates (~25 – 70 cm/1000 years) and, except for MC22A and MC13A, have modern core tops as indicated by radiocarbon (fraction

modern (Fm) >1) (Table S1, Fig. S4). The records span the last  $\sim 500 - 2,250$  years (Fig. 2, Data S1-3, Fig. S5-14).

# Rapid Transmission of Common Era Surface Climate Trends to Depth

5

10

15

20

25

30

35

40

All but one planktic  $\delta^{13}$ C records from cores with Fm >1 show a sharp decrease in recently-deposited sediments (Fig. S9, S11, S12), reflecting the oceanic uptake of isotopically light anthropogenic carbon released by fossil fuel burning since the early  $19^{th}$  century (17). The rapid decrease of planktic  $\delta^{13}$ C near the top of MC13A suggests its top is modern despite its relatively low Fm value. Eight out of the 10 benthic records from cores with modern tops have lowest values near their tops. Of these, the  $\delta^{13}$ C decrease is significant relative to the post-1850 period in six records (Fig. S7, S12). The amplitude of the  $\delta^{13}$ C decrease in the benthic records ranges from about 0.1 to 0.4 ‰, consistent with modelled amplitude (18). The finding of low core-top  $\delta^{13}$ C in the benthic records confirms an important role for AMOC in sequestering anthropogenic carbon into the deep ocean.

Most planktic  $\delta^{18}O$  records from cores with modern tops show a decrease since the early  $20^{th}$  century, suggesting warming and/or freshening (Fig. 2, S8, S10). At least half of the benthic  $\delta^{18}O$  records also show a decrease during this time period (Fig. 2, S6), although the signals are smaller than in the planktic records, and a statistical test, discussed below, was used to establish their significance. Most benthic and planktic records extending into the MCA appear to show a  $\delta^{18}O$  increase across the MCA-LIA transition, suggesting cooling and/or increasing salinity. However, at the shallowest site (MC28A,  $\sim 1000$  m) the benthic  $\delta^{18}O$  decreases across the MCA-LIA transition and through most of the LIA. The amplitude of the MCA-LIA benthic  $\delta^{18}O$  increase is also relatively small at the next deepest site (MC26A,  $\sim 1200$  m) compared to the deeper sites.

To determine whether and when significant changes in the mean of  $\delta^{18}$ O time series occurred, we computed the change points of the  $\delta^{18}$ O records, adapting a method that accounts for age uncertainty and data variability and was previously used to detect AMOC strength change (19) (Methods). We divided the  $\delta^{18}$ O records into post-1850 and pre-1850 datasets, and conducted change point analyses on each time interval. For the post-1850 interval, we excluded MC22A, which does not have a modern core top. For the pre-1850 dataset, we only included the six cores with Bayesian ensemble median ages older than 1200 CE (Table S1). For each core and foraminifera species, we computed the average  $\delta^{18}O$  difference before and after the change point if the significance test was passed (Fig. 3). Key findings from these change point analyses are: (1) most planktic (15 out of 20) and half of the benthic (5 out of 10) records show statistically significant 20<sup>th</sup> century  $\delta^{18}$ O decreases; (2) most planktic (10 out of 15) and benthic (5 out of 6) records show statistically significant  $\delta^{18}$ O increases across the MCA-LIA transition; and (3) of the records with a significant  $\delta^{18}O$  increase across the MCA-LIA transition, the average ages of the benthic  $\delta^{18}$ O change points are in a narrow range, ~1346 ± 49 CE, whereas the planktic  $\delta^{18}$ O change points occur across an  $\sim$ 600-year range, between 1100 and 1700 CE (average  $\sim$ 1357  $\pm$ 216 CE) (Data S4). The large range of planktic change points may reflect earlier cooling at our northern than southern sites (Fig. S15). Bioturbation, coupled with higher abundances of the planktic foraminifera near the tops of the cores, may have resulted in a small (~ 2-3 cm) downcore shift of the recent planktic  $\delta^{18}O$  decrease (Figs. S16-17), implying that the post-1850 change point may have been more recent than implied by our analyses. Composites of raw  $\delta^{18}$ O data from all cores on their median Bayesian ages confirm larger variability in the planktic  $\delta^{18}$ O than benthic  $\delta^{18}$ O records (Fig. S14).

We interpret the  $20^{th}$ -century  $\delta^{18}O$  decrease recorded in the planktic records as rapid warming and freshening of subpolar surface and near-surface North Atlantic waters, consistent with planktic faunal changes in the same cores ((20), Fig. S18) and instrumental evidence indicating surface or near-surface warming and freshening trends since the 1950s both basin-wide (21, 22) and locally (23) (Fig. S19). The smaller magnitude of the benthic (0.04 - 0.22 ‰) than planktic  $\delta^{18}O$  decreases (0.06 - 0.43 ‰) in the late  $20^{th}$  century (Fig. 3B) is consistent with a recent, rapid, high-amplitude surface signal that was diluted by mixing with older waters in transit to the deep core sites. Thus, the corresponding trends of decreasing  $\delta^{18}O$  and direct observations of recent warming and freshening imply that we can use the  $\delta^{18}O$  signals in these cores to infer past changes related to seawater density.

With the exception of the MC25A G. inflata record, average planktic  $\delta^{18}O$  was  $\sim 0.05$  to 0.25 % higher after the MCA-LIA change point than before it (Fig. 3A). At sites deeper than 1300 m, the mean benthic  $\delta^{18}O$  is 0.05 to 0.14 % higher after the MCA-LIA change point than before it. If these changes were driven by temperature, the benthic  $\delta^{18}O$  increases would correspond to 0.2 - 0.6 °C average cooling (14). The smoothed benthic composite record suggests that on average, the deep sites (> 1300 m) increased by  $\sim 0.1$ %, or cooled by  $\sim 0.5$ °C, similar to the change point results from individual records (Fig. 3A, S14). While temperature likely dominated the benthic  $\delta^{18}O$  increases at these deep sites (> 1300 m), we cannot rule out that the  $\delta^{18}O$  of one or more water masses influencing these sites changed across this transition.

Rapid transfer of surface signals to our deep core sites is consistent with young water mass ages at the sites (~35-65 years; Fig. S2) implied by a global inversion of modern oceanographic data (10). We infer that the greater range in the timing of change points in the planktic records across the MCA-LIA transition (1076 – 1712 CE), compared to the benthic records (1275 – 1395 CE) (Fig. S15) is due to several factors, including larger seasonal and depth-habitat variations of planktic foraminifera, the time-transgressive nature of surface change, larger temporal variability in the surface (for example the meandering of zonal fronts on seasonal-interannual-decadal timescales), and a potential contribution due to bioturbation coupled with planktic foraminifera abundance changes (Supplementary text). Furthermore, the narrower range of benthic than planktic change points is the expected consequence of interior ocean mixing that damps surface variability. Globally-averaged temperature anomalies, for example, exhibit their greatest interannual variability above 500 m depth, but the deeper ocean is more representative of the longer-term ocean heat gain (24). Thus, the benthic records integrate the surface variability and more reliably record the overall timing of the MCA-LIA cooling/salinification.

# **Arctic Amplification of MCA-LIA Cooling**

5

10

15

20

25

30

35

40

45

We compare our  $\delta^{18}O$  records with results from an ocean model inversion (25) (referred to as OPT-0015 hereinafter), which fits an empirical ocean circulation model to modern-day tracer observations, historical deep-sea temperature in the 1870s (26), and global-mean Ocean2k sea surface temperature (SST) reconstructed for the Common Era (6) (Supplementary text). The OPT-0015 inversion solves for the three-dimensional evolution of temperature throughout the Common Era under the assumption of a fixed, modern-day ocean circulation. In the inversion, SST is allowed to vary regionally in order to fit the subsurface constraints. We extracted the OPT-0015 model temperature simulated at the model grid nearest our cores and converted the temperature into  $\delta^{18}O$  changes using empirical calibrations (14). The model exhibits temporal trends consistent with those in the foraminiferal  $\delta^{18}O$  records of the surface and the deeper sites (Figs. 2, 4), showing both LIA cooling and  $20^{th}$ -century warming.

To compare data and model change points, we first obtained model variability by computing 100-year moving averages in the surface mixed layer and at 2000 m depth, and then performed change point analyses on the moving averages (Fig. S20). For both the surface and deep sites, the post-1850 change point in the model and data are within error, especially considering chronological uncertainty in our records (Fig. 3B). On the other hand, there is a large data-model change point mismatch in the timing of significant LIA cooling/salinification, with the model change points occurring ~350 years before the average benthic and planktic change points (Fig. 3A). This occurs because the model was constrained with the Ocean2k SSTs (25), which contain cooling before and during the MCA, and which the model then faithfully reproduces. In contrast, other independent estimates of the timing of the LIA from regions proximal to our study area yield ages that are more consistent with the change point derived from our benthic  $\delta^{18}$ O records (~1346 ± 49 CE), such as an Arctic temperature reconstruction (27) (~1258 ± 2 CE) and Greenland ice cap growth records (28) (~1353 ± 9 CE).

The model inversion suggests that for multi-centennial variability in the pre-1850s, including the MCA-LIA transition, temperature change in the deep sea (>1000 m) was greater than the upper ocean (500-1000 m) (Fig. 4A). The reason that the deep sea cools more than the upper ocean during the simulated LIA is related to Arctic amplification of the LIA cooling, which is present in the SST inversion (25) and was also simulated in the Community Earth System Model-Last Millennium Ensemble (29). Thus, cooling in the Nordic Seas where the overflows originated was greater than in waters formed south of the sills (25, 29). With an active AMOC, larger cold anomalies from the Nordic Seas are transmitted to depth via the overflows. Contrasting with the MCA-LIA cooling, modern warming is (thus far) concentrated in the upper ocean, both in observations and in OPT-0015 (Fig. 3B and 4B). During the MCA – LIA transition, the deep ocean had sufficient time to record the cooling which lasted ~ 600 years, whereas the time interval of 20th century warming was shorter. Thus, the core sites, having average water mass ages of 40-70 years (modern, Fig. S2), have not yet had sufficient time to fully record the warming at depth, and anomalies at depth will always lag those at the surface unless warming ceases.

# MCA - LIA SPMW Freshening/Warming

5

10

15

20

25

30

35

40

45

The model inversion suggests a large cooling across the MCA-LIA transition that is not evident in the benthic  $\delta^{18}$ O data of the two shallowest sites (MC28A and 26A) (Fig. 2). This benthic data-model mismatch likely reflects MCA-LIA oceanographic changes (i.e., changes in circulation, seawater  $\delta^{18}$ O, salinity), that were not considered in the inversion. The shallowest site, MC28A, which shows a trend of decreasing  $\delta^{18}$ O from the MCA through the end of the LIA, is currently within the high salinity zone of SPMW (Fig. 1), which has been diluted by mixing with LSW and overflows (Figs. S1-2). It is possible that a cooling trend at site MC28A was compensated by freshening that is not considered in the model, and that the temperaturerelated  $\delta^{18}$ O increase at MC26A was also dampened by freshening. Fresh, low- $\delta^{18}$ O polar waters may have been incorporated into SPMW, which most affects the two shallowest sites. This hypothesis is consistent with evidence of increased sea-ice export from the Arctic that began at ~1300 CE and continued through the LIA (8, 30, 31). SPMW freshening during the LIA was also inferred downstream of the eastern subtropical gyre (32). Alternatively, or in addition, a greater contribution of a fresher, lower- $\delta^{18}$ O upper LSW relative to SPMW to our shallow sites could have resulted in the observed  $\delta^{18}O$  decrease. Given that overflows entrain less dense waters during their descent along the ridge (9), it is possible that all our core sites were fresher during the LIA than MCA. If the LIA cooling from the OPT-0015 inversion  $(0.4 - 0.6 \,^{\circ}\text{C})$  is assumed

accurate, cooling at all but one site would have been partially compensated by a decrease in  $\delta^{18}\text{Osw}$  (freshening) (Fig. S21). Such a freshening at depth may also explain why the benthic  $\delta^{18}\text{O}$  data do not record the higher amplitude of the MCA-LIA deep cooling compared to the surface suggested by OPT-0015 (Figs. 3, 4, S20). However, we cannot rule out the possibility that the MCA-LIA trend of decreasing benthic  $\delta^{18}\text{O}$  at our shallow site reflects warming of SPMW. Possible warming mechanisms include greater transport of warm subtropical waters to the SPMW formation regions (33, 34) or a weakening AMOC, which results in upper ocean subsurface warming due to reduced convection and exchange with the overlying cold atmosphere (35).

## 10 Conclusion

5

15

20

25

30

35

Whereas modern warming is surface intensified, typically in the upper ~700 m (2), our model simulation posits that on longer time scales, temperature change in the deep subpolar North Atlantic exceeds that in the upper ocean, consistent with polar amplification of temperature change and an active overflow. Our data provide strong support for a persistent role of the AMOC in transferring anomalous upper ocean heat and freshwater to depth during the last ~1,200 years. The records indicate a deep ocean that cooled and lost heat during the LIA, implying that the heat was transferred to the upper ocean and atmosphere (25). Thus, the ocean acted to dampen MCA- LIA surface change much like it is dampening surface warming during the industrial era. The model simulation we used assumes that the intensity of the AMOC was unchanged from the modern. If the AMOC has declined during the 20<sup>th</sup> century as several studies suggest (36, 37), and AMOC during most of the Common Era was stronger, then the pre-20<sup>th</sup>-century AMOC may have played a larger role in transferring surface climate signals to depth than in the modern.

## References and Notes

- 1. R. Neukom et al., Nat Geosci. 12, 643-649 (2019), doi:10.1038/s41561-019-0400-0.
- 2. S. Levitus et al., Geophys. Res. Lett. 39, L10603 (2012). doi:10.1029/2012GL051106.
- 3. G. A. Meehl, J. M. Arblaster, J. T. Fasullo, A. Hu, K. E. Trenberth, *Nat. Clim. Chang.* **1**, 360–364 (2011). doi:10.1038/nclimate1229.
- 4. X. Chen, K. K. Tung, *Science* **345**, 897-903 (2014). doi:10.1126/science.1254937.
- 5. M.-J. Messias, H. Mercier, *Commun. Earth Environ.* **3**, 118 (2022). doi:10.1038/s43247-022-00443-4.
- 6. H. v. McGregor et al., Nat. Geosci. 8, 671–677 (2015). doi:10.1038/ngeo2510.
- 7. B. Dickson et al., *Nature* **416**, 832-835 (2002). doi:10.1038/416832a.
- 8. P. Moffa-Sánchez et al., *Paleoceanogr. Paleoclimatol.* **34**, 1399-1436 (2019). doi:10.1029/2018PA003508.
  - 9. H. R. Langehaug et al., *Paleoceanography*. **31**, 399–415 (2016). doi:10.1002/2015PA002920.
  - 10. G. Gebbie, P. Huybers, J Phys. Oceanogr. 42, 291-305 (2012). doi:10.1175/JPO-D-11-043.1.
- 40 11. T. Rossby, L. Chafik, L. Houpert, *Geophys. Res. Lett.* **47**, e2020GL087456 (2020). doi:10.1029/2020GL087456.

- 12. L. Jonkers, S. van Heuven, R. Zahn, F. J. C. Peeters, *Paleoceanography* **28**, 164-174 (2013). doi:10.1002/palo.20018.
- 13. A. Rebotim et al., *J. Micropalaeontol.* **38**, 113-131 (2019). doi:10.5194/jm-38-113-2019.
- 14. T. M. Marchitto et al., *Geochim. Cosmochim. Acta.* **130**, 1-11 (2014). doi:10.1016/j.gca.2013.12.034.

5

- 15. G. A. Schmidt, G. R. Bigg, E. J. Rohling, Global Seawater Oxygen-18 Database v1.22 (1999). (available at https://data.giss.nasa.gov/o18data/)
- 16. N. P. McKay, J. Emile-Geay, D. Khider, *Geochronology* **3**, 149-169 (2021). doi:10.5194/gchron-3-149-2021.
- 17. C. D. Keeling, *Environ. Int.* **2**, 229-300 (1979). doi:10.1016/0160-4120(79)90005-9.
  - 18. M. Eide, A. Olsen, U. S. Ninnemann, T. Eldevik, *Global Biogeochem. Cycles* **31**, 492-514 (2017). doi:10.1002/2016GB005472.
  - 19. L. Caesar, G. D. McCarthy, D. J. R. Thornalley, N. Cahill, S. Rahmstorf, *Nat. Geosci.* **14**, 118-120 (2021). doi:10.1038/s41561-021-00699-z.
- 20. P. T. Spooner et al., *Geophys. Res. Lett.* **47**, e2020GL087577 (2020). doi:10.1029/2020GL087577.
  - 21. R. Curry, C. Mauritzen, Science 308, 1772-1774 (2005). doi:10.1126/science.1109477.
  - 22. A. R. Friedman, G. Reverdin, M. Khodri, G. Gastineau, *Geophys. Res. Lett.* **44**, 1866-1876 (2017). doi:10.1002/2017GL072582.
- 23. Marine and Freshwater Research Institute Iceland, Marine measurements around Iceland. https://sjora.hafro.is/ (2022).
  - 24. D. Roemmich et al., Nat. Clim. Chang. 5, 240-245 (2015). doi:10.1038/nclimate2513.
  - 25. G. Gebbie, P. Huybers, Science 363, 70-74 (2019), doi:10.1126/science.aar8413.
  - 26. D. Roemmich, W. J. Gould, J. Gilson, *Nat. Clim. Chang.* **2**, 425-428 (2012). doi:10.1038/nclimate1461.
  - 27. N. P. McKay, D. S. Kaufman, Sci. Data 1, 140026 (2014). doi:10.1038/sdata.2014.26.
  - 28. M. B. Osman et al., *Nat. Geosci.* **14**, 756-761 (2021). doi:10.1038/s41561-021-00818-w.
  - 29. B. L. Otto-Bliesner et al., *Bull. Am. Meteorol Soc.* **97**, 935-954 (2016). doi:10.1175/BAMS-D-14-00233.1.
- 30. M. W. Miles, C. S. Andresen, C. v. Dylmer, *Sci. Adv.* **6**, eaba4320 (2020). doi:10.1126/sciadv.aba4320.
  - 31. M. Alonso-Garcia et al., Clim. Past 13, 317-331 (2017). doi:10.5194/cp-13-317-2017.
  - 32. A. Morley et al., *Earth Planet. Sci. Lett.* **308**, 161-171 (2011). doi:10.1016/j.epsl.2011.05.043.
- 33. D. Desbruyères, L. Chafik, G. Maze, *Commun. Earth Environ.* **2**, 48 (2021), doi:10.1038/s43247-021-00120-y.
  - 34. D. J. R. Thornalley, H. Elderfield, I. N. McCave, *Nature* 457, 711-714 (2009). doi:10.1038/nature07717.

- 35. Z. Liu et al., Science 325, 310-314 (2009), doi:10.1126/science.1171041.
- 36. D. J. R. Thornalley et al., *Nature* **556**, 227-230 (2018). doi:10.1038/s41586-018-0007-4.
- 37. L. Caesar, S. Rahmstorf, A. Robinson, G. Feulner, V. Saba, *Nature* **556**, 191-196 (2018). doi:10.1038/s41586-018-0006-5.
- 38. A. Bower, H. Furey, *J. Geophys. Res. Oceans* **122**, 6989–7012 (2017). doi:10.1002/2017JC012698.
- 39. M. I. García-Ibáñez et al., *Prog. Oceanogr.* 135, 18-36 (2015). doi:10.1016/j.pocean.2015.03.009.
- 40. T. P. Boyer et al., World Ocean Atlas 2018 (Temperature and salinity). *NOAA National Centers for Environmental Information* (2018). (available at https://www.ncei.noaa.gov/products/world-ocean-atlas).
- 41. R. Schlitzer, Ocean Data View (2021). (available at https://odv.awi.de/).
- 42. P. Moffa-Sánchez, A. Born, I. R. Hall, D. J. R. Thornalley, S. Barker, *Nat. Geosci.* **7**, 275-278 (2014). doi:10.1038/ngeo2094.

**Acknowledgments:** We thank the WHOI Seafloor Samples Repository for curating the samples, and WHOI NOSAMS for radiocarbon analyses. We thank K. Pietro and S. Wang for technical assistance.

**Funding:** This work was funded by NSF grants OCE-2031929 (to G.G. and D.W.O.) and OCE-1304291 (to D.W.O. and D.J.R.T.) and by WHOI's Edna McConnell Clark Foundation Fund (to D.W.O.). W.L. was supported by the WHOI Postdoctoral Scholar Program, with funding provided by the Weston Howland Jr. Postdoctoral Scholarship, and by NSF OCE-2114579 (to D.W.O).

# **Author contributions:**

25 Conceptualization: DWO, GG

5

10

15

20

30

Methodology: WL, DWO, GG

Investigation: WL, DWO, GG, DJRT

Visualization: WL, DWO

Funding acquisition: DWO, GG, DJRT, WL

Project administration: DWO

Supervision: DWO, GG

Writing – original draft: WL

Writing – review & editing: WL, DWO, GG, DJRT

**Competing interests:** The authors declare no competing interests.

**Data and materials availability:** Source data for Figs. 1-3, S6-S15 are provided in the supplementary materials. The raw radiocarbon, isotope data and R-scripts to reproduce the results are publicly available at both the National Center for Environmental Data (https://www.ncei.noaa.gov/access/paleo-search/study/38185) and Zenodo repository (URL will be open to public upon acceptance).

# **Supplementary Materials**

Materials and Methods

Supplementary Text

Figs. S1 to S21

Tables S1

Data S1-S4

References (43–48)

15

20

25

5

Fig. 1. Locations of eleven EN539 multicores along with schematic illustrations of ocean circulations (A), sea surface temperature (B), sea surface salinity (C), temperature (D), salinity (E), and  $\delta^{18}O_{\text{calcite}}$  (F) sections along the eastern flank of Reykjanes Ridge. The isopycnal layers are shown in dashed lines in F), with the 27.8 kg/m<sup>3</sup> isopycnal defining the upper boundary of the ISOW plume (38). The ocean circulation paths were adapted from ref. (39), with thin red arrows showing warm salty surface Atlantic waters, thin green arrow showing cold fresh surface water sourced from Arctic, and thick dashed lines showing deep overflow pathways. Temperature and salinity data are the average of six decadal climatologies from 1955 to 2017 from the World Ocean Atlas 2018 (40). The  $\delta^{18}O_{\text{calcite}}$  section was converted from an oceanographic data inversion (10) using empirical calibrations (14). The figures were generated using Ocean Data View software (41). SPG: Subpolar Gyre; NAC: North Atlantic Current; EGC:

East Greenland Current; ISOW: Iceland-Scotland Overflow Water; DSOW: Denmark Strait Overflow Water; LSW: Labrador Sea Water; SPMW: Subpolar Mode Water.

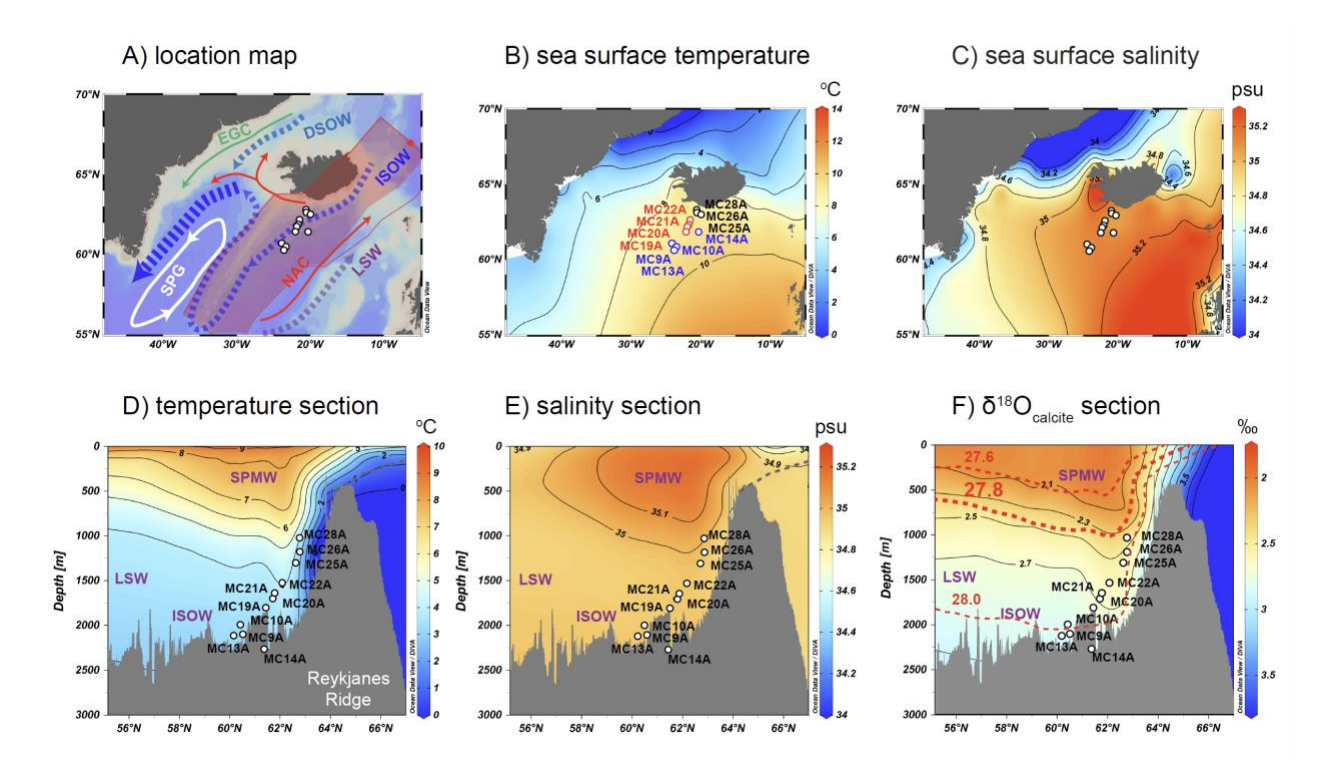


Fig. 2. Planktic and benthic  $\delta^{18}$ O records compared with global mean surface air temperature (GMST) history (1) and temperature anomalies from the OPT-0015 inversion model (25). A) Global mean surface air temperature anomalies with respect to 1961–1990 CE. B)-D) 11 foraminiferal  $\delta^{18}$ O records arranged by increasing core water depth. Thick colored lines correspond to the median  $\delta^{18}$ O ensemble member, and colored shading shows the 90% highest-density probability ranges determined by R software package "geoChronR" (16) (Methods). To compare the modelled temperature trends (black dashed lines, OPT-0015) to the  $\delta^{18}$ O changes, we scaled a 1°C decrease to correspond to a 0.22%  $\delta^{18}$ O increase (14). Thick color-coded arrows indicate mean ensemble change point ages where they are significant, and cyan-colored bars

5

denote the ranges of these ages. Benthic records in MC28A, 26A, 25A were generated on *U. peregrina*, and the other benthic records were generated on *C. wuellerstorfi*.

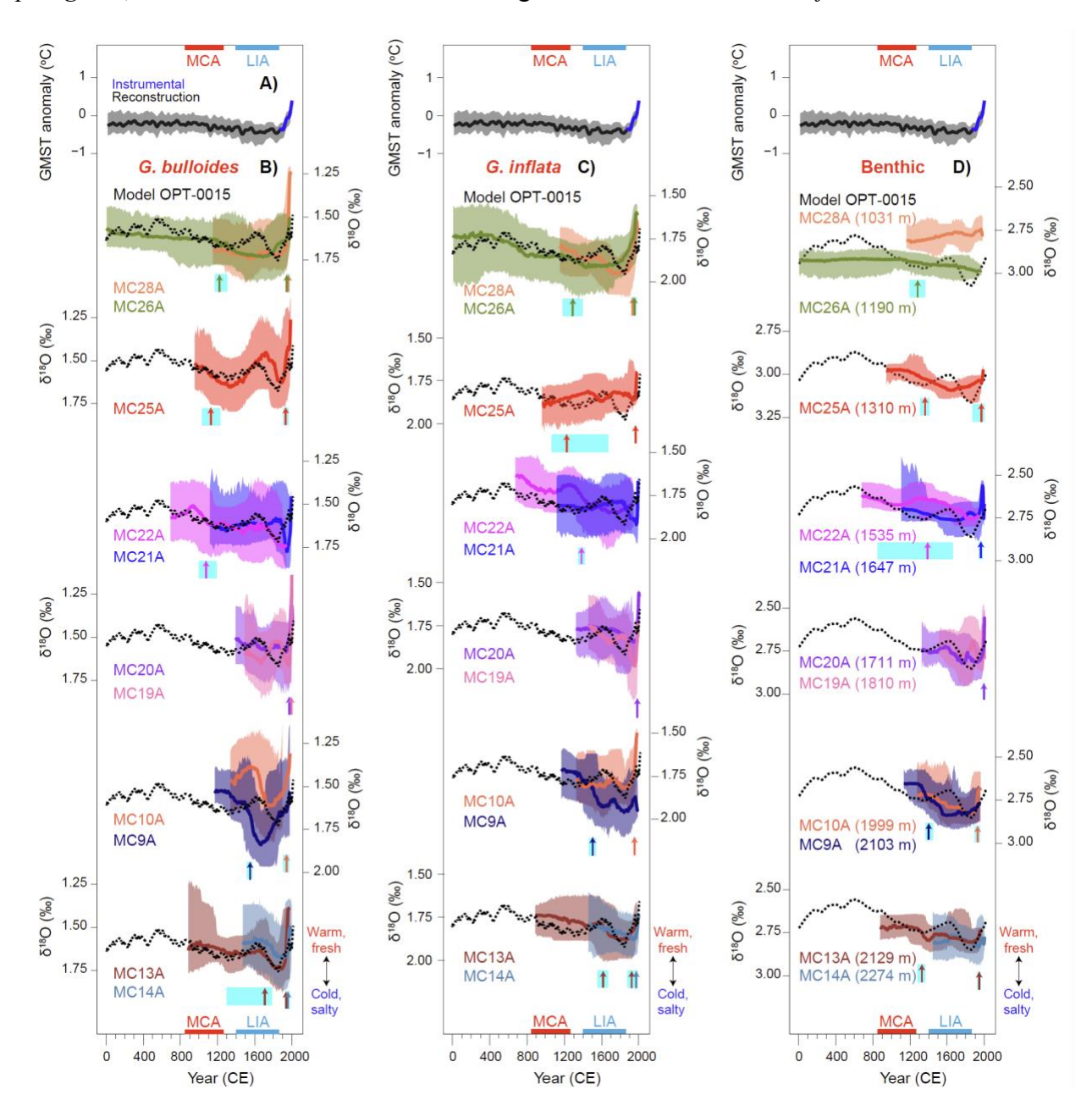


Fig. 3. Change point (CP) estimates vs.  $\delta^{18}$ O differences (after minus before the CP) in both  $\delta^{18}$ O records and OPT-0015 inversion for the MCA-LIA transition (pre-1850 dataset) (A) and industrial era (post-1850 dataset) (B). Note that the y-axes are reversed. Points below the zero dashed line in A) imply colder saltier LIA conditions; points above the zero dashed line in B) imply warmer fresher post-1950s conditions. In the benthic records, open circles denote U.

peregrina, closed circles denote *C. wuellerstorfi*. The *G. inflata*  $\delta^{18}$ O record of nearby core RAPiD-17-5P is from ref. (42).

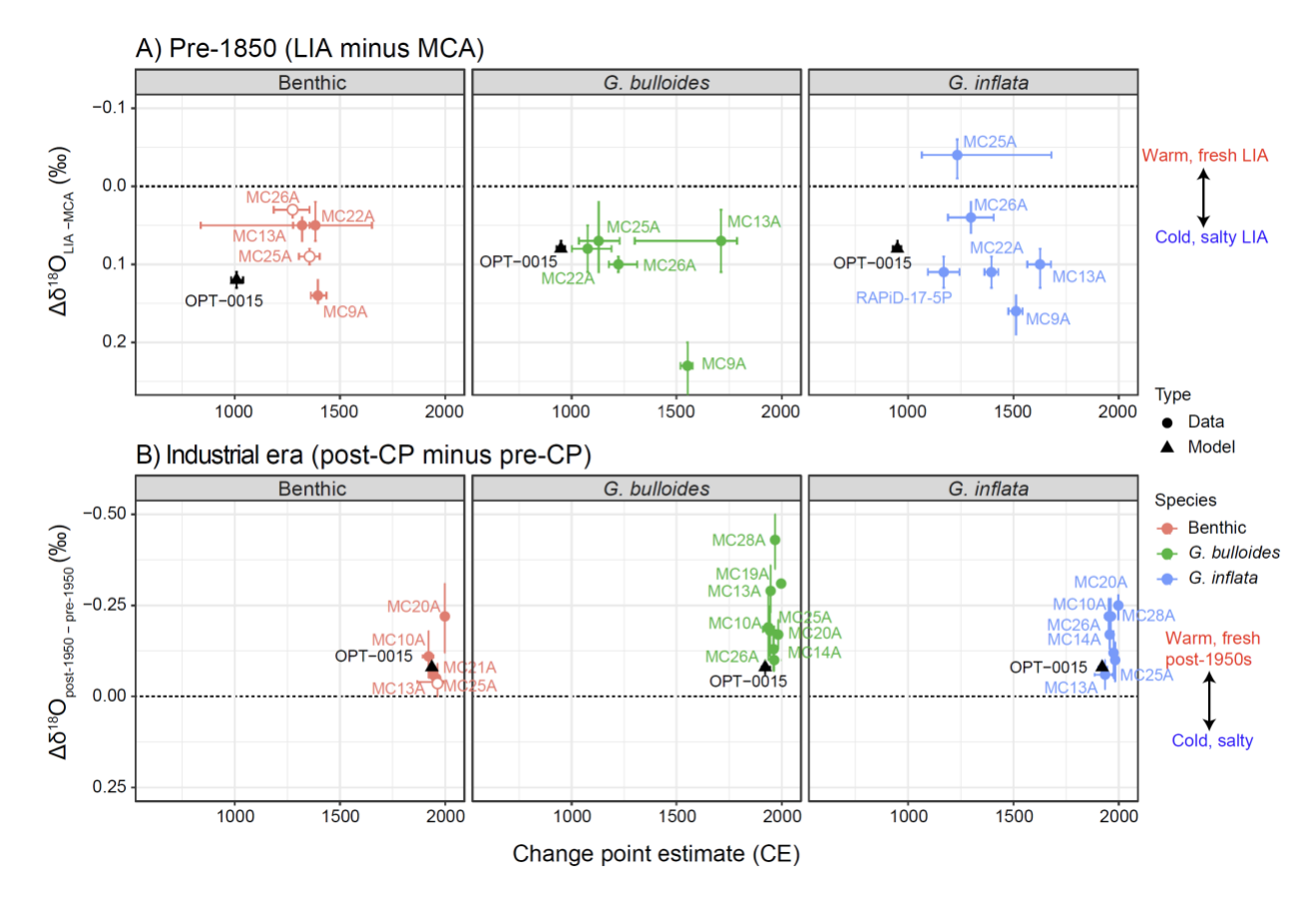


Fig. 4. Anomalous temperature evolution south of Iceland (grid box of 61.5°N, 20.5°W) from the OPT-0015 inversion (25) during the last 2,000 years (A) and from 1850 to 2015 CE (B).

